Downward Mapping of High-Latitude Ionospheric Electric Fields to the Ground

C. G. PARK

Radioscience Laboratory, Stanford University, Stanford, California 94305

The main purpose of this paper is to draw attention to the important but long neglected problem of electrical coupling between the ionosphere and the lower atmosphere. A numerical technique is used to calculate electric fields and currents between 0- and 150-km altitude produced by large-scale horizontal electric fields known to exist in the polar cap and auroral ionosphere. A two-dimensional model assuming a flat earth and a vertical geomagnetic field is used. The results show that horizontal electric fields in the ionosphere map down to ~10 km with little attenuation, in agreement with previous authors' results. In addition, these horizontal ionospheric electric fields should cause significant modulations of vertical electric fields down to the earth's surface. The effects of conductivity irregularities in the ionosphere, stratosphere, and troposphere are also examined. Localized conductivity enhancements associated with aurora are expected to produce a horizontal electric field of up to a few millivolts per meter at ~30-km altitude in the absence of any horizontal field in the ionosphere. These conductivity enhancements have less than a 1% effect on the vertical electric field on the ground. The effects of stratospheric and tropospheric irregularities are negligible at large heights but become important below ~20 km. Their magnitude depends on how the ratio between the local resistivity and the height-integrated columnar resistance is altered.

INTRODUCTION

Much progress has been made in recent years toward understanding the electrical structure of the ionosphere and the magnetosphere. This progress was made possible in large part by a number of recently developed electric field measurement techniques, such as electrostatic probes flown on satellites [e.g., *Maynard and Heppner*, 1970; *Gurnett*, 1970], on rockets [e.g., *Mozer and Bruston*, 1967; *Aggson*, 1969], and on balloons [e.g., *Mozer and Serlin*, 1969]; drift measurements of whistler ducts [e.g., *Carpenter et al.*, 1972] and barium clouds [e.g., *Haerendel and Lüst*, 1970; *Wescott et al.*, 1970]; and incoherent scatter radars [e.g., *Woodman*, 1970; *Banks et al.*, 1973; *Evans*, 1972]. Observed electric fields show large spatial and temporal variations depending on their origin. Solar-wind-induced convection produces fields of tens of millivolts per meter in the polar cap and auroral zone ionosphere. During geomagnetic storms and substorms (processes through which the magnetosphere explosively releases its energy to the atmosphere), peak amplitudes of up to 100 mV/m are observed in the auroral ionosphere. These impulsive fields also spread to middle latitudes with amplitudes of several millivolts per meter. The atmospheric dynamo generates electric fields of the order of 1 mV/m centered at middle latitudes. Owing to large conductivities along the geomagnetic field, electric fields at and above ionospheric heights are nearly perpendicular to the geomagnetic field (large electric fields in the direction of the geomagnetic field can be produced by plasma instabilities, but we will not consider such fields in this paper). These electric fields clearly play fundamental roles in ionospheric and magnetospheric dynamics. The question that we wish to consider in this paper is how these fields map downward and affect atmospheric electric fields at low altitudes. We will limit our discussion to high-latitude convection and auroral electric fields. The dynamo electric field has been discussed by *Volland* [1972].

It is generally accepted that thunderclouds drive upward currents, charging the ionosphere to a potential of some 200 kV with respect to the earth [e.g., *Dolezalek*, 1972]. In 'fair-weather' regions, return currents to the earth produce vertical electric fields of the order of 100 V/m near the ground. In such a picture of the 'global circuit' it has been a general practice to assume an equipotential ionosphere, sometimes referred to as the 'potential equalizing layer.' We now realize that the ionosphere must be treated not only as a finite conductivity medium that can support imposed electric fields but also as an active electric generator. Ionospheric electric fields of 100 mV/m or less may appear to be insignificant, but since these fields extend over large areas, they can easily produce potential drops of tens of kilovolts in the ionosphere. On occasion, such potential drops may exceed the average ionosphere-to-earth potential difference. Even dynamo electric fields of the order of 1 mV/m can produce a potential difference of tens of kilovolts on a global scale. It is clear that these large-scale generators in the ionosphere must be included in a proper model of the global circuit. The construction of such a three-dimensional global model is beyond the scope of this paper. Here we will use two-dimensional models to investigate how certain types of ionospheric electric fields map down to the ground and how they compare with the fields produced by the thunderstorm-driven circuit. We will also examine how electric field mapping is affected by conductivity irregularities in the ionosphere, stratosphere, and troposphere.

Several authors have recently discussed downward mapping of ionospheric electric fields. *Kellogg and Weed* [1969], *Mozer* [1971], and *Volland* [1972] considered simple cases of isotropic atmosphere in which conductivity is described by a single exponential function of altitude. *Dejnakarintra* [1974], *Park and Dejnakarintra* [1974*a*], and *Chiu* [1974] included conductivity anisotropy and used analytical solutions for each horizontally stratified slab in multiple-slab models of the atmosphere. *Boström* [1974] also included conductivity anisotropy, but he used numerical solutions and extended the analysis to time-varying and moving sources in the ionosphere. All previous mapping techniques have two limitations in common: (1) the source potential in the ionosphere is assumed to vary sinusoidally with horizontal distance, and (2) the conductivities are assumed to vary with altitude only. In theory, the first limitation is not serious, because any source potential distribution can be Fourier-analyzed. In practice, however, it proves to be a laborious task to Fourier-analyze the source, to

map each Fourier component separately, and then to sum up the results. In this paper we adopt numerical techniques that allow direct calculations of electric fields and currents between 0- and 150-km altitude for any arbitrary potential distribution specified at the upper boundary and for any arbitrary conductivity distribution, including horizontal gradients. The results generally support the conclusion of previous authors that ionospheric electric fields map down to low altitudes very efficiently. The next section describes the mapping theory, followed by the results of calculations and concluding remarks.

THEORY

The basic equations to be solved are

$$\nabla \cdot \mathbf{J} = 0 \tag{1}$$

$$\mathbf{J} = \boldsymbol{\sigma}\mathbf{E} \tag{2}$$

$$\mathbf{E} = -\nabla\Phi \tag{3}$$

where $\mathbf{J}$ is the electric current density, $\mathbf{E}$ is the electric field, $\boldsymbol{\sigma}$ is the conductivity tensor, and Φ is the electric potential. Since we are interested only in high-latitude phenomena in this paper, we assume a flat earth with the geomagnetic field directed vertically downward. In a Cartesian coordinate system with the z axis pointing upward we can write

$$J_x = \sigma_p E_x + \sigma_H E_y$$

$$J_y = \sigma_p E_y - \sigma_H E_x$$

$$J_z = \sigma_0 E_z$$

where σ_0, σ_p, and σ_H are the specific, Pedersen, and Hall conductivities, respectively. By means of these relationships, equation (1), (2), and (3) can be combined to yield

$$\sigma_p \frac{\partial^2\Phi}{\partial x^2} + \sigma_p \frac{\partial^2\Phi}{\partial y^2} + \sigma_0 \frac{\partial^2\Phi}{\partial z^2} + \left(\frac{\partial\sigma_p}{\partial x} - \frac{\partial\sigma_H}{\partial y}\right)\frac{\partial\Phi}{\partial x} + \left(\frac{\partial\sigma_H}{\partial x} + \frac{\partial\sigma_p}{\partial y}\right)\frac{\partial\Phi}{\partial y} + \frac{\partial\sigma_0}{\partial z}\frac{\partial\Phi}{\partial z} = 0$$

The azimuthal symmetry of this problem allows us to reduce it to a two-dimensional problem with no loss of generality but with considerable savings of computation time. Thus we let $\partial/\partial y = 0$ to obtain

$$\sigma_p \frac{\partial^2\Phi}{\partial x^2} + \sigma_0 \frac{\partial^2\Phi}{\partial z^2} + \frac{\partial\sigma_p}{\partial x}\frac{\partial\Phi}{\partial x} + \frac{\partial\sigma_0}{\partial z}\frac{\partial\Phi}{\partial z} = 0 \tag{4}$$

The boundary conditions to be satisfied by this differential equation include $\Phi = 0$ at $z = 0$ and $\Phi(x)$ specified at the upper boundary in the ionosphere. The other set of boundary conditions is best specified in terms of $\Phi(z)$ at $x = \pm\infty$. In order to find these boundary conditions we construct our models in such a way that both $\partial\Phi/\partial x$ at $z = 150$ km and $\partial\sigma/\partial x$ vanish as $x \to \pm\infty$. Under these conditions, J_x also vanishes as $x \to \pm\infty$, and $\Phi(\pm\infty, z)$ can be easily calculated from

$$\Phi(\pm\infty, z) = \Phi(\pm\infty, z_u)\left(\int_0^z \frac{dz}{\sigma_0} \Big/ \int_0^{z_u} \frac{dz}{\sigma_0}\right)$$

where z_u is the altitude of the upper boundary.

In order to facilitate numerical solution of (4) we introduce a new variable $p = \arctan(\alpha x)$, which has a finite range $-\pi/2$ to $+\pi/2$, as x varies from $-\infty$ to $+\infty$. Equation (4) then becomes

$$\frac{\alpha^2}{(1+\alpha^2x^2)^2}\sigma_p\frac{\partial^2\Phi}{\partial p^2} - \frac{2\alpha^3 x}{(1+\alpha^2x^2)^2}\sigma_p\frac{\partial\Phi}{\partial p} + \frac{\alpha}{1+\alpha^2x^2}\frac{\partial\sigma_p}{\partial x}\frac{\partial\Phi}{\partial p} + \sigma_0\frac{\partial^2\Phi}{\partial z^2} + \frac{\partial\sigma_0}{\partial z}\frac{\partial\Phi}{\partial z} = 0 \tag{5}$$

Equation (5) can now be solved by a standard numerical technique. We set up a grid in the p-z space, assume an initial distribution of Φ, and keep making corrections through a line iteration scheme [e.g., *Diaz et al.*, 1958] until a satisfactory accuracy is achieved. The value of α is adjusted in order to obtain the maximum density of grid points in the region of special interest. Once Φ is known, E and J are easily obtained from (2) and (3).

RESULTS

We will first consider cases involving no horizontal conductivity gradients. The effects of conductivity irregularities will be examined later in this section. In all our calculations we specify a potential distribution at 150-km altitude as the upper boundary condition. Figure 1 shows conductivity profiles intended to represent the undisturbed polar region (taken from work of *Park and Dejnakarintra* [1974*a*]). The columnar resistance $R = \int dz/\sigma_0 = 1.4 \times 10^{17}\ \Omega/m^2$, and if we assume a uniform ionospheric potential of $\Phi = 200$ kV with respect to the earth, a vertical air-earth current of $1.4 \times 10^{-12}\ A/m^2$ flows everywhere. The vertical electric field $E_z = (1/\sigma_0)(\Phi/R)$ is inversely proportional to σ_0 of Figure 1.

We now examine how horizontal electric fields in the ionosphere map down to lower altitudes. We assume a constant horizontal electric field E_{x0} confined between $x = -(L/2)$ and $x = +(L/2)$ at 150-km altitude as shown by the solid curve in Figure 2. Below 150 km, E_x decreases with decreasing altitude, but the rate of decrease is a strong function of the scale size L. This is clearly indicated by the dashed curves in Figure 2, which are plots of E_x versus x at $z = 30$ km for selected values of L. The scales are normalized to the assumed values of L and E_{x0} at $z = 150$ km. As L decreases, E_x suffers increasing attentuation and becomes more smeared out in the x direction. Figure 3 shows how E_x at $x = 0$ varies with altitude for $L = 20$ and 100 km.

It is clear that ionospheric electric fields with $L \gtrsim 100$ km

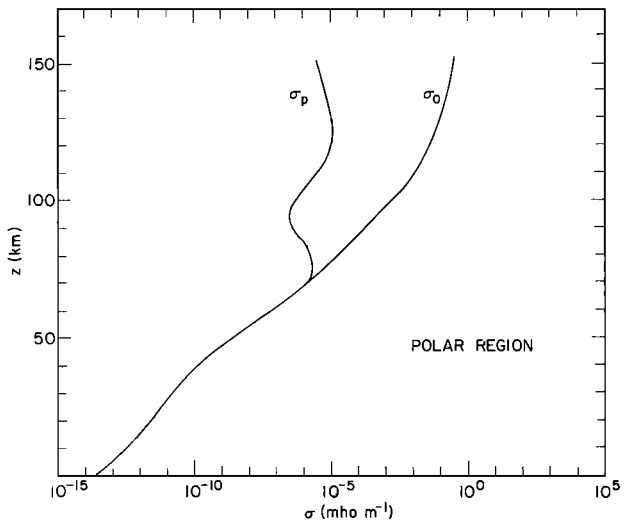

Fig. 1. Model conductivity profile representing the quiet time polar region; σ_0 is the conductivity along the geomagnetic field, and σ_p is the Pedersen conductivity.

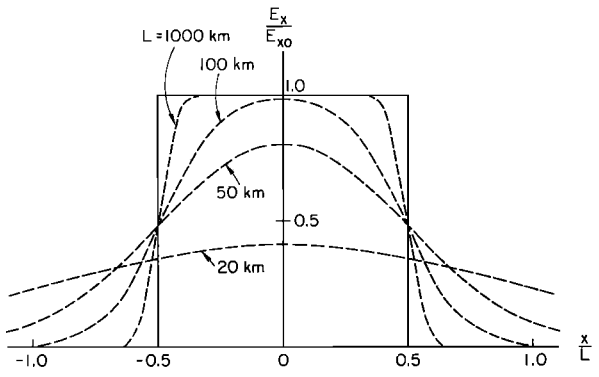

Fig. 2. Normalized horizontal electric field at z = 30 km plotted against normalized horizontal distance. The step function variation shown in the solid curve represents the ionospheric source electric field at z = 150 km.

can reach 10-km altitude with little attenuation, in agreement with the conclusions of several earlier studies [*Kellogg and Weed*, 1969; *Mozer*, 1971; *Chiu*, 1974; *Park and Dejnakarintra*, 1974*a*; *Boström and Fahleson*, 1974]. Below 10 km, E_x decreases rapidly even for large-scale fields because of the canceling effect of electric fields arising from induced charges on the earth's surface. Such a canceling effect is confined to the lowest few kilometers, because the induced fields suffer severe attenuation as they map upward in the direction of increasing conductivity. It is useful to remember that electric fields are transmitted more efficiently in the direction of decreasing conductivity. Thus in the earth's atmosphere, where the conductivity increases rapidly with altitude, downward field mapping is much more efficient than upward mapping. (See the treatment of the upward mapping problem by *Park and Dejnakarintra* [1973, 1974*b*].)

Before discussing numerical results for the vertical electric field we can see the relationship between horizontal and vertical fields through the simple physical picture illustrated in Figure 4. If we demand that the line integral $\oint \mathbf{E}\cdot d\mathbf{l} = 0$ around the rectangular path and assume that $E_{xg} = 0$ along the ground path, then obviously, E_{z1} and E_{z2} must be adjusted so as to accommodate the ionospheric horizontal field E_{xi}.

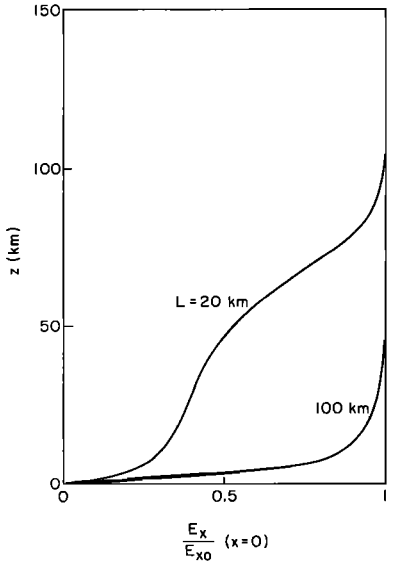

Fig. 3. Plots showing altitude variations of horizontal electric field at x = 0 for an ionospheric source field confined within L = 20 and 100 km.

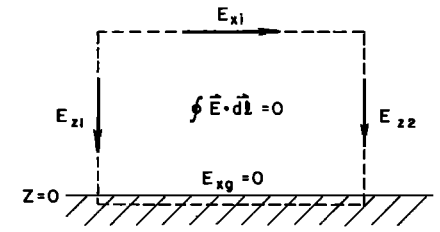

Fig. 4. Relationships between horizontal and vertical electric fields.

Figure 5 shows the results for vertical electric field E_z. At the top of the figure is the potential distribution at z = 150 km, corresponding to the horizontal field assumed to exist there in Figure 2. The lower part of the figure shows E_z at z = 0, normalized to the potential drop $\Delta\Phi$, for selected values of L. For $|x| \gg 0.5L$, E_z is proportional to the overhead ionospheric potential. Near the region of ionospheric potential gradient the imposed Φ variation is accurately reproduced by the E_z curves for $L > 100$ km. For smaller values of L the curves become more smeared out.

Dawn-dusk convection electric field. Figure 6 is a sketch of the simplified plasma circulation pattern in the northern polar ionosphere that results from solar wind–magnetosphere interactions [e.g., *Axford*, 1969]. Since the plasma flow velocity $\mathbf{v} = (\mathbf{E} \times \mathbf{B})/B^2$ is perpendicular to $\mathbf{E} = -\nabla\Phi$ above ~120-km altitude, the flow lines in Figure 6 also represent equipotential contours [e.g., *Hines*, 1964]. Thus the ionospheric potential varies in the dawn to dusk direction as sketched in an idealized form at the top of Figure 7. Electrostatic probes flown on polar-orbiting satellites show that the basic pattern illustrated here is a persistent feature of the polar ionosphere, although many details may change from pass to pass depending upon the conditions in interplanetary space and the magnetosphere [*Heppner*, 1972*a*, *b*; *Cauffman and Gurnett*, 1972; *Gurnett and Frank*, 1973]. In Figure 7 we have assumed a potential drop of Φ_{DD} = 100 kV from the dawn side to the dusk side boundary of

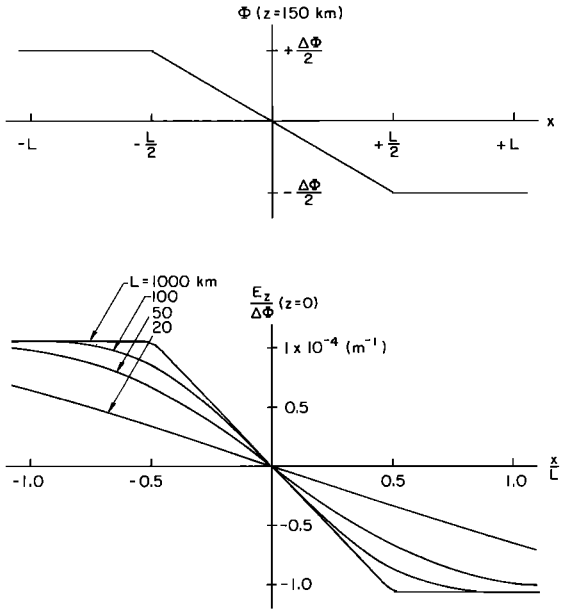

Fig. 5. (Top) The assumed ionospheric potential distribution. (Bottom) The corresponding vertical electric field on the ground (normalized to the assumed ionospheric potential difference) for several values of L within which the ionospheric potential variation is confined.

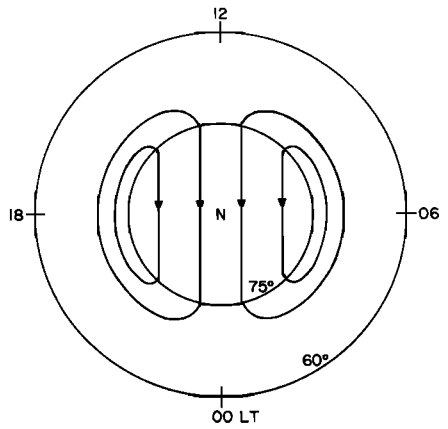

Fig. 6. Sketch of plasma flow pattern in the high-latitude ionosphere in a latitude–local time coordinate system. The flow lines are also equipotential lines.

the polar cap. The values of Φ_{DD} deduced from satellite measurements of E_x range from ~50 to ~250 kV [*Heppner*, 1972*b*; *Gurnett and Frank*, 1973]. Equatorward of the polar cap boundary at 75° magnetic latitude the potential is assumed to recover linearly across the auroral belt to the global average ionospheric potential of 200 kV with respect to the earth [e.g., *Dolezalek*, 1972].

The two lower curves in Figure 7 show the results of calculations for E_x at z = 30 km and for E_z at z = 0. The E_z curve closely follows the variation in ionospheric potential, and the E_x curve is nearly identical in shape and magnitude to the assumed ionospheric potential gradients. These results could have been predicted from Figures 2, 3, and 5, since the scale sizes involved here are measured in hundreds and thousands of kilometers.

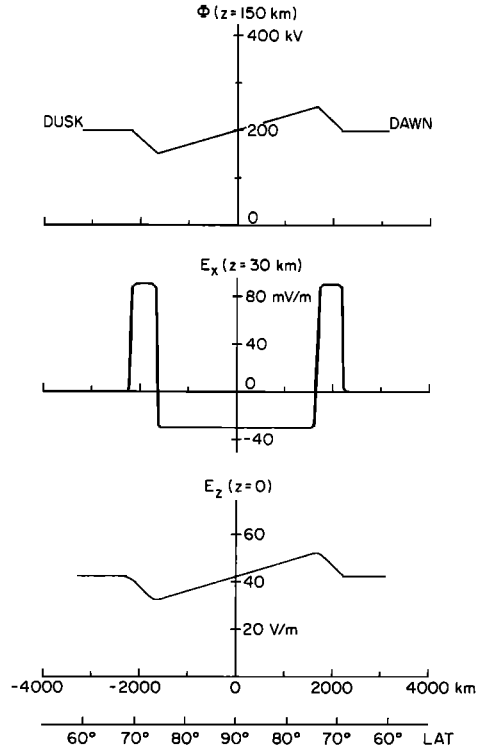

Fig. 7. (Top) Typical dawn to dusk variation in ionospheric potential across the polar cap. (Middle) Calculated horizontal electric field at z = 30 km. (Bottom) Calculated vertical electric field at z = 0.

Electrostatic probes flown on balloons near 30-km altitude have reported horizontal electric fields that are consistent with the predictions of Figure 7 [*Mozer and Manka*, 1971; *Ogawa et al.*, 1974; *Mozer et al.*, 1974].

Figure 7 predicts a significant magnetospheric influence on vertical atmospheric electric field near the polar cap boundary. For the parameters used in this example a ground station on the dawn side boundary should report a field strength ~1.7 times greater than that reported by a station on the dusk side. This factor would be 1.3 and 4.3 for Φ_{DD} = 50 and 250 kV, respectively. (The absolute values of E_z in Figure 7 are not to be taken very seriously, because they depend on the vertical conductivity profile near the ground. However, the variations in E_z expressed in terms of ratios do not depend on the conductivity profile.) A sudden increase in Φ_{DD}, associated with a southward turning of the interplanetary magnetic field or a magnetospheric substorm [*Gurnett and Akasofu*, 1974], should cause a sudden increase in E_z on the dawn side and a simultaneous decrease on the dusk side. No simultaneous measurements of this kind have been reported. In single-station studies the diurnal variation expected from the above picture would tend to be obscured by temporal variations in Φ_{DD} and the location of the polar cap boundary as well as in the global average potential of the ionosphere. Nevertheless, it is somewhat puzzling that no clear evidence of dawn-dusk asymmetry has been found in the diurnal variation of E_z and J_z measured at polar latitude stations [e.g., *Kasemir*, 1972; *Cobb*, 1974].

Auroral electric fields. Ionospheric electric fields associated with aurora have been measured by a number of techniques, including incoherent scatter radar [e.g., *Banks et al.*, 1973], rocket-borne probes [e.g., *Aggson*, 1969], and barium releases [e.g., *Wescott et al.*, 1970]. In the night side auroral oval, electric fields are greatly enhanced during active aurora. Such enhanced fields are not always accompanied by similar enhancements in the dawn-dusk polar cap fields, indicating that there are other sources of electric fields associated with auroral substorms in addition to the solar-wind-driven convection. Furthermore, these auroral electric fields are not limited to the region of visible, discrete aurora but extend over the 'diffuse' auroral arc, ~5°–10° wide in magnetic latitude. Within the diffuse arc the electric field is directed predominantly in the north-south direction and may reach 100 mV/m or more in amplitude. The meridional field is directed equatorward in the morning sector, driving a westward Hall current, and poleward in the evening sector, driving an eastward Hall current. The east-west component of the electric field is typically a factor of 3–10 less than the north-south component. This component, unlike the north-south component, shows anticorrelation with ionospheric conductivity [*Banks et al.*, 1974; *Mozer et al.*, 1973]. Thus in mapping east-west electric fields the effects of nonzero source impedance must be taken into account. For north-south fields the assumption of an ideal voltage source appears to be justified [*Mozer et al.*, 1973; P. M. Banks, private communication, 1975].

Electric fields associated with auroral substorms also spread to middle latitudes and produce important plasma dynamic effects in the plasmasphere and the ionosphere [e.g., *Carpenter and Park*, 1973]. In middle latitudes the field strength is typically a few millivolts per meter, but since the field spreads over large areas, potential differences of tens of kilovolts can exist in the middle latitude ionosphere. Such middle latitude problems, however, will not be discussed in this paper.

During an intense auroral event a meridional field of ~100 mV/m may appear over ~10° in magnetic latitude (~1100-km

distance), producing an ionospheric potential difference of ~100 kV. The mapping of such a potential gradient is similar to the L = 1000 km case illustrated in Figures 2 and 5. It is clear from Figure 2 that the horizontal fields should map down to balloon altitudes of ~30 km or less. This has been confirmed by a number of balloon flights in the auroral zone [e.g., *Mozer et al.*, 1973; *Mozer and Lucht*, 1974; *Kelley and Mozer*, 1975]. Figure 5 shows that E_z measured on the ground should closely follow the variation in overhead ionospheric potential. If we assume an average ionospheric potential of 200 kV, we predict a 1.67:1 change in E_z as we cross the auroral oval in a north-south direction. (It is more meaningful to consider ratios rather than absolute values of E_z, because the latter depend on conductivities near the ground.)

Auroral effects on E_z have not been clearly demonstrated by ground-based measurements. Some observers reported on cases in which changes in E_z were apparently correlated with aurora [e.g., *Freier*, 1961; *Olson*, 1971; *Lobodin and Paramonov*, 1972] (see also the discussion of earlier work by *Israël* [1973]), while others reported no correlation after examining a considerable amount of data [e.g., *Shaw and Hunsucker*, 1974].

Effects of Conductivity Irregularities

Thus far we have assumed no horizontal gradients in conductivity. We will now consider how electric field mapping is affected by the presence of conductivity irregularities in the ionosphere, stratosphere, and troposphere. Figure 8 illustrates schematically three different types of irregularity. Each type of irregularity is characterized by conductivity enhancement factors that can be represented by Gaussian functions of x and z. Since very few experimental data are available on these irregularities, particularly below ~80 km, we will adopt reasonable ranges of values for each parameter to see how important the effects of irregularities are compared to other factors. To examine the effects of irregularities we assume a uniform ionospheric potential of 200 kV at z = 150 km so that the calculated E_x can be attributed entirely to the irregularity. The effects on E_z can be easily seen by a comparison with the simple case of a horizontally stratified medium in which E_z is inversely proportional to σ_0.

Ionospheric irregularity. This type of irregularity may be produced by precipitating particles and associated Bremsstrahlung X rays, such as those in an active aurora. Enhanced particle precipitation occurs in the entire band of diffuse aurora, some 5°–10° wide in latitude, but there may also be smaller-scale structures within the diffuse auroral arc. The enhancement factor is described by

$$f = 1 + (\lambda - 1) \exp\left[-\left(\frac{x}{x_0}\right)^2\right] \qquad z \geq z_i$$

and

$$f = 1 + (\lambda - 1) \exp\left[-\left(\frac{x}{x_0}\right)^2\right] \exp\left[-\left(\frac{z_i - z}{z_0}\right)^2\right] \qquad z < z_i$$

These irregularities have no appreciable effect on the columnar resistance or on the air-earth current density. Obviously, for the same vertical current density the potential drop should be less inside an irregularity, where conductivities are higher. This gives rise to horizontal electric fields directed away from the center of such an irregularity. Figure 9 shows E_x at z = 10, 20, and 30 km. The parameters of the irregularity in this example are λ = 100, z_i = 40 km, z_0 = 7.5 km, and x_0 = 250 km. Calculations have been repeated for the same upper boundary condition but for different parameters characterizing the conductivity irregularity. The results are summarized in Table 1, where the maximum amplitude $E_{x,\max}$ is tabulated for each selected altitude level. The case labeled I-2 is the case illustrated in Figure 9. Except in the somewhat extreme case I-4 the magnitude of E_x due to conductivity irregularities is a few millivolts per meter, about 1 order of magnitude less than what would be expected from typical auroral electric fields in the ionosphere.

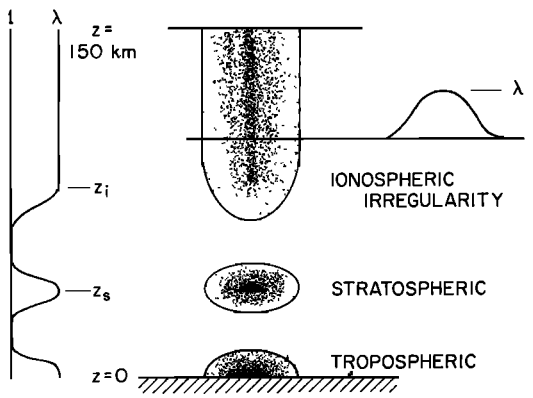

Fig. 8. Sketch illustrating the three different kinds of conductivity irregularities considered in this paper.

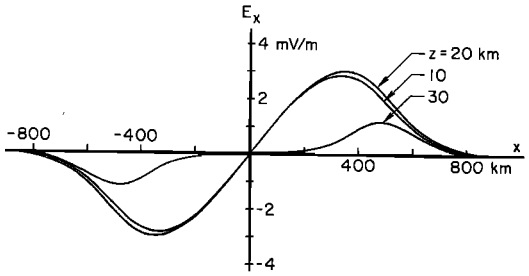

Fig. 9. Horizontal electric fields produced by an ionospheric conductivity irregularity (see text for details).

Table 1 also shows the maximum effect on E_z at z = 0. The irregularity, centered at x = 0, would slightly decrease the columnar resistance and increase J_z and E_z at z = 0. This change in E_z at z = 0 and x = 0 is tabulated in the last column of Table 1 as a percentage increase over E_z at z = 0 and x = $\pm\infty$. The effect is typically less than 1%.

We conclude from these sample calculations that the conductivity irregularities associated with aurora do not significantly affect downward mapping of auroral electric fields in the ionosphere. However, care must be exercised in interpreting balloon measurements of E_x of less than a few millivolts per meter.

Stratospheric irregularity. The enhancement factor in this case is described by

$$f = 1 + (\lambda - 1) \exp\left[-\left(\frac{x}{x_0}\right)^2\right] \exp\left[-\left(\frac{z_s - z}{z_0}\right)^2\right]$$

The results for two different sets of parameters are shown as S-1 and S-2 in Table 1. Electric fields around these irregularities have similar spatial variations as in the case of an ionospheric irregularity, but their magnitudes are larger. The effects on E_z measured on the ground are still negligible, because the columnar resistance and the vertical current density are not significantly perturbed.

TABLE 1. Effects of Conductivity Irregularities

Case	λ	z_i or z_s, km	z_0, km	x_0, km	$E_{z,\max}$, mV/m z = 30 km	z = 20 km	z = 10 km	$\Delta E_{z,\max}$, % z = 0
I-1	100	70	15	250	0.3	0.4	0.4	+0.07
I-2	100	40	7.5	250	1.2	3.0	2.9	+0.73
I-3	100	70	15	25	2.7	1.7	1.9	+0.05
I-4	100	40	10	25	10.2	51.2	91.0	+2.30
S-1	10	30	10	250	0.9	6.3	22.6	+6.2
S-2	5	30	10	50	3.7	25.6	74.0	+3.7
T-1	2		20	250	1.0	4.7	14.3	−4.6
T-2	2		10	250	0.9	6.3	33.2	−13
T-3	2		5	250	0.6	4.1	32.0	−25
T-4	2		2	250	0.3	1.9	14.6	−35
T-5	10		10	250	6.6	42.3	126.	−36
T-6	10		5	250	2.8	19.0	142.	−65
T-7	10		2	250	0.9	6.0	47.6	−80

Tropospheric irregularity. We represent the enhancement factor in this case by

$$f = 1 + (\lambda - 1) \exp\left[-\left(\frac{x}{x_0}\right)^2\right] \exp\left[-\left(\frac{z}{z_0}\right)^2\right]$$

Conductivity irregularities near the ground may significantly change the columnar resistance between the ground and the ionosphere as well as local conductivities. If the columnar resistance is decreased by the presence of a conductivity enhancement, the resulting increase in vertical current causes the potential to drop faster with decreasing altitude above the enhanced conductivity region. This gives rise to horizontal electric fields directed toward the center of such an irregularity. Figure 10*a* shows E_x at z = 10 and 20 km for λ = 2, x_0 = 250 km, and z_0 = 5 km (case T-3 in Table 1). Figure 10*b* shows E_z at z = 0 for the same case. Cases T-1–T-7 in Table 1 summarize the results for different values of λ and z_0. As we increase z_0, an action which means increasing the vertical extent of the irregularity, we predict larger horizontal fields but smaller effects on vertical fields. The latter result is due to the fact that E_z depends on the ratio between local conductivity and columnar resistance. Obviously, if $z_0 \to \infty$, the shape of the vertical conductivity profile will remain unchanged, and therefore E_z will also remain unaffected in the first order.

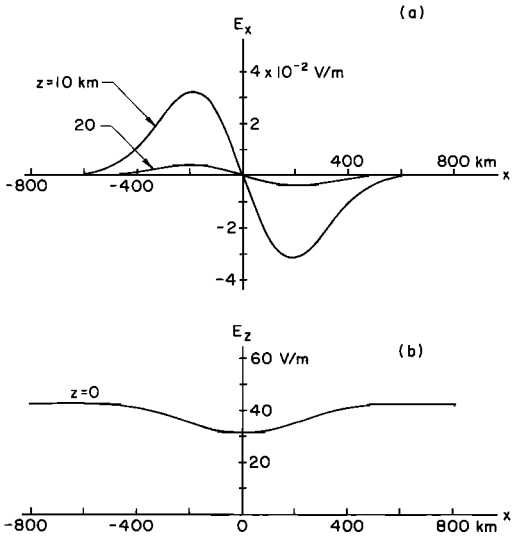

Fig. 10. (*a*) Horizontal electric fields produced by a conductivity irregularity near the ground. (*b*) Vertical electric fields on the ground. (See text for details.)

For the range of values considered here, horizontal fields of a few millivolts per meter can be produced at z = 30 km due to irregularities at lower altitudes. These fields increase rapidly with decreasing altitude. Therefore it is clearly advantageous to gain maximum altitude when horizontal fields of ionospheric origin are measured on balloons or aircraft. Vertical fields near the ground can be significantly affected by localized conductivity irregularities. In such cases, additional measurements of conductivity and/or air-earth current would be needed to interpret the measurements.

In all the cases of Table 1 we assumed a uniform ionospheric potential of 200 kV at z = 150 km. The tabulated values of $E_{x,\max}$ vary linearly with this assumed ionospheric potential, but the percentage effects on E_z are independent of this potential.

CONCLUDING REMARKS

We conclude that atmospheric electric fields at low altitudes can be significantly modulated by electric fields known to exist in the ionosphere. The solar-terrestrial influence on atmospheric electricity is an important area that needs to be explored through increased experimental efforts and theoretical modeling. It appears to be particularly important in view of recent interest in possible solar-terrestrial effects on the weather [e.g., *Markson*, 1971; *Wilcox et al.*, 1973; *Roberts and Olson*, 1973]. Electric fields provide a direct link between the ionosphere and the troposphere, but the role of atmospheric electricity in many tropospheric processes is only poorly known at present.

Our results generally support the ideas behind balloon measurements of horizontal ionospheric electric fields, but at the same time, they point out a need for caution when the measured field strength is less than a few millivolts per meter. Near the ground, horizontal fields of ionospheric origin are expected to be far below detectable limits. On the other hand, measurements of vertical electric fields along with air-earth currents and conductivities at spaced stations may provide useful information on electrical coupling between the ionosphere and the troposphere.

Acknowledgments. I want to thank D. L. Carpenter, T. F. Bell, and H. Dolezalek for careful reading of the manuscript. This research was supported by the National Science Foundation, Atmospheric Sciences Section, under grant DES74-20084. I also thank the National Center for Atmospheric Research, which is sponsored by the National

Science Foundation, for the computing used in this research. Figure 4 was suggested by one of the referees.

The Editor thanks M. C. Kelley and H. Volland for their assistance in evaluating this paper.

REFERENCES

Aggson, T. L., Probe measurements of electric fields in space, in *Atmospheric Emissions*, edited by B. M. McCormac and A. Omholt, p. 305, Van Nostrand Reinhold, New York, 1969.

Axford, W. I., Magnetospheric convection, *Rev. Geophys. Space Phys.*, *7*, 421, 1969.

Banks, P. M., J. R. Doupnik, and S.-I. Akasofu, Electric field observations by incoherent scatter radar in the auroral zone, *J. Geophys. Res.*, *78*, 6607, 1973.

Banks, P. M., C. L. Rino, and V. B. Wickwar, Incoherent scatter radar observations of westward electric fields and plasma densities in the auroral ionosphere, 1, *J. Geophys. Res.*, *79*, 187, 1974.

Boström, R., Ionosphere-magnetosphere coupling, in *Magnetospheric Physics*, edited by B. M. McCormac, p. 45, D. Reidel, Dordrecht, Netherlands, 1974.

Boström, R., and U. Fahleson, Vertical propagation of time-dependent electric fields in the atmosphere and ionosphere, paper presented at 5th International Conference on Atmospheric Electricity, Garmisch-Partenkirchen, West Germany, Sept. 2–7, 1974.

Carpenter, D. L., and C. G. Park, On what ionospheric workers should know about the plasmapause-plasmasphere, *Rev. Geophys. Space Phys.*, *11*, 133, 1973.

Carpenter, D. L., K. Stone, J. C. Siren, and T. L. Crystal, Magnetospheric electric fields deduced from drifting whistler paths, *J. Geophys. Res.*, *77*, 2819, 1972.

Cauffman, D. P., and D. A. Gurnett, Satellite measurements of high latitude convection electric fields, *Space Sci. Rev.*, *13*, 369, 1972.

Chiu, Y. T., Self-consistent electrostatic field mapping in the high-latitude ionosphere, *J. Geophys. Res.*, *79*, 2790, 1974.

Cobb, W. E., Atmospheric electric measurements at the South Pole, paper presented at 5th International Conference on Atmospheric Electricity, Garmisch-Partenkirchen, West Germany, Sept. 2–7, 1974.

Dejnakarintra, M., A theoretical study of electrical coupling between the troposphere, ionosphere and magnetosphere, *Tech. Rep. 3454-3*, Radiosci. Lab., Stanford Electron. Lab., Stanford Univ., Stanford, Calif., 1974.

Diaz, J. B., R. F. Clippinger, B. Friedman, E. Isaacson, and R. Richtmyer, Partial differential equations, in *Handbook of Automation, Computation and Control*, vol. 1, edited by E. M. Grabbe, S. Ramo, and D. E. Wooldridge, pp. 14–64, John Wiley, New York, 1958.

Dolezalek, H., Discussion of the fundamental problem of atmospheric electricity, *Pure Appl. Geophys.*, *100*, 8, 1972.

Evans, J. V., Measurements of horizontal drifts in the *E* and *F* regions at Millstone Hill, *J. Geophys. Res.*, *77*, 2341, 1972.

Freier, G. D., Auroral effects on the earth's electric field, *J. Geophys. Res.*, *66*, 2695, 1961.

Gurnett, D. A., Satellite measurements of dc electric fields in the ionosphere, in *Particles and Fields in the Magnetosphere*, edited by B. M. McCormac, p. 239, D. Reidel, Dordrecht, Netherlands, 1970.

Gurnett, D. A., and S.-I. Akasofu, Electric and magnetic field observations during a substorm on February 24, 1970, *J. Geophys. Res.*, *79*, 3197, 1974.

Gurnett, D. A., and L. A. Frank, Observed relationships between electric fields and auroral particle precipitation, *J. Geophys. Res.*, *78*, 145, 1973.

Haerendel, G., and R. Lüst, Electric fields in the ionosphere and magnetosphere, in *Particles and Fields in the Magnetosphere*, edited by B. M. McCormac, D. Reidel, Dordrecht, Netherlands, 1970.

Heppner, J. P., Polar cap electric field distributions related to the interplanetary magnetic field direction, *J. Geophys. Res.*, *77*, 4877, 1972*a*.

Heppner, J. P., Electric field variations during substorms—Ogo 6 measurements, *Planet. Space Sci.*, *20*, 1475, 1972*b*.

Hines, C. O., Hydromagnetic motions in the magnetosphere, *Space Sci. Rev.*, *3*, 342, 1964.

Israël, H., *Atmospheric Electricity*, vol. 2, *Fields, Charges Currents*, p. 403, translated from German, Israel Program for Scientific Translations, Jerusalem, 1973.

Kasemir, H. W., Atmospheric electric measurements in the Arctic and Antarctic, *Pure Appl. Geophys.*, *100*, 70, 1972.

Kelley, M. C., and F. S. Mozer, Simultaneous measurement of the horizontal components of the earth's electric field in the atmosphere and in the ionosphere, *J. Geophys. Res.*, *80*, 3275, 1975.

Kellogg, P. J., and M. Weed, Balloon measurements of ionospheric electric fields, in *Planetary Electrodynamics*, vol. 2, edited by S. C. Coroniti and J. Hughes, p. 431, Gordon and Breach, New York, 1969.

Lobodin, T. V., and N. A. Paramonov, Variation of atmospheric electric field during aurorae, *Pure Appl. Geophys.*, *100*, 167, 1972.

Markson, R., Considerations regarding solar and lunar modulation of geophysical parameters, atmospheric electricity, and thunderstorms, *Pure Appl. Geophys.*, *84*, 161, 1971.

Maynard, N. C., and J. P. Heppner, Variations in electric fields from polar orbiting satellites, in *Particles and Fields in the Magnetosphere*, edited by B. M. McCormac, p. 247, D. Reidel, Dordrecht, Netherlands, 1970.

Mozer, F. S., Balloon measurements of vertical and horizontal electric fields, *Pure Appl. Geophys.*, *84*, 32, 1971.

Mozer, F. S., and P. Bruston, Electric field measurements in the auroral ionosphere, *J. Geophys. Res.*, *72*, 1109, 1967.

Mozer, F. S., and P. Lucht, The average auroral zone electric field, *J. Geophys. Res.*, *79*, 1001, 1974.

Mozer, F. S., and R. H. Manka, Magnetospheric electric field properties deduced from simultaneous balloon flights, *J. Geophys. Res.*, *76*, 1967, 1971.

Mozer, F. S., and R. Serlin, Magnetospheric electric field measurements with balloons, *J. Geophys. Res.*, *74*, 4739, 1969.

Mozer, F. S., F. H. Bogott, and B. Tsurutani, Relations between ionospheric electric fields and energetic trapped and precipitating electrons, *J. Geophys. Res.*, *78*, 630, 1973.

Mozer, F. S., W. D. Gonzalez, F. H. Bogott, M. C. Kelley, and S. Schutz, High-latitude electric fields and the three-dimensional interaction between the interplanetary and the terrestrial magnetic fields, *J. Geophys. Res.*, *79*, 56, 1974.

Ogawa, T., Y. Tanaka, A. Huzita, and M. Yasuhara, Three dimensional electric fields and currents in the stratosphere, paper presented at 5th International Conference on Atmospheric Electricity, Garmisch-Partenkirchen, West Germany, Sept. 2–7, 1974.

Olson, D. E., The evidence for auroral effects on atmospheric electricity, *Pure Appl. Geophys.*, *84*, 118, 1971.

Park, C. G., and M. Dejnakarintra, Penetration of thundercloud electric fields into the ionosphere and magnetosphere, 1, Middle and subauroral latitudes, *J. Geophys. Res.*, *78*, 6623, 1973.

Park, C. G., and M. Dejnakarintra, The effects of magnetospheric convection on atmospheric electric field in the polar cap, paper presented at 5th International Conference on Atmospheric Electricity, Garmisch-Partenkirchen, West Germany, Sept. 2–7, 1974.

Park, C. G., and M. Dejnakarintra, Thundercloud electric fields in the ionosphere, paper presented at 5th International Conference on Atmospheric Electricity, Garmisch-Partenkirchen, West Germany, Sept. 2–7, 1974*b*.

Roberts, W. O., and R. H. Olson, New evidence for effects of variable solar corpuscular emission on the weather, *Rev. Geophys. Space Phys.*, *11*, 731, 1973.

Shaw, G. E., and R. D. Hunsucker, A study of possible correlation between fair-weather electric field and auroral activity, paper presented at 5th International Conference on Atmospheric Electricity, Garmisch-Partenkirchen, West Germany, Sept. 2–7, 1974.

Volland, H., Mapping of the electric field of the *Sq* current into the lower atmosphere, *J. Geophys. Res.*, *77*, 1961, 1972.

Wescott, E. M., J. D. Stolarik, and J. P. Heppner, Auroral and polar cap electric fields from barium releases, in *Particles and Fields in the Magnetosphere*, edited by B. M. McCormac, p. 229, D. Reidel, Dordrecht, Netherlands, 1970.

Wilcox, J. M., P. H. Scherrer, L. Svalgaard, W. O. Roberts, and R. H. Olson, Solar magnetic sector structure: Relation to circulation of the earth's atmosphere, *Science*, *180* (4082), 185, 1973.

Woodman, R. H., Vertical drift velocities and east-west electric fields at the magnetic equator, *J. Geophys. Res.*, *74*, 1205, 1970.

(Received April 9, 1975;
accepted June 25, 1975.)